Journal of Cellular Biochemistry

# The intranuclear PEX domain of MMP involves proliferation, migration, and metastasis of aggressive adenocarcinoma cells

| | |
|---|---|
| Journal: | *Journal of Cellular Biochemistry* |
| Manuscript ID | JCB-17-1144.R1 |
| Wiley - Manuscript type: | Research Article |
| Date Submitted by the Author: | n/a |
| Complete List of Authors: | Okusha, Yuka; Okayama University Graduate School of Medicine, Dentistry and Pharmaceutical Sciences<br>Eguchi, Takanori; Okayama University Graduate School of Medicine, Dentistry and Pharmaceutical Sciences,<br>Sogawa, Chiharu; Okayama University Graduate School of Medicine, Dentistry and Pharmaceutical Sciences<br>Okui, Tatsuo ; Okayama University Graduate School of Medicine, Dentistry and Pharmaceutical Sciences, Department of Oral and Maxillofacial Surgery and Biopathology<br>Nakano, Keisuke; Okayama University Graduate School of Medicine, Dentistry and Pharmaceutical Sciences, Department of Oral Pathology and Medicine<br>Okamoto, Kuniaki; Okayama University Graduate School of Medicine, Dentistry and Pharmaceutical Sciences<br>Kozaki, Ken-ichi; Okayama University Graduate School of Medicine, Dentistry and Pharmaceutical Sciences |
| Keywords: | nuclear MMP, PEX domain, non-proteolytic MMP, cancer metastasis, tumor stroma |
| | |

# The intranuclear PEX domain of MMP involves proliferation, migration, and metastasis of aggressive adenocarcinoma cells

Yuka Okusha,[1] Takanori Eguchi,[1,2,*] Chiharu Sogawa,[1] Tatsuo Okui,[3] Keisuke Nakano,[2,4] Kuniaki Okamoto,[1] and Ken-ichi Kozaki[1]

[1]Department of Dental Pharmacology,

[2]Advanced Research Center for Oral and Craniofacial Sciences,

[3]Department of Oral and Maxillofacial Surgery,

[4]Department of Pathology and Medicine,

Graduate School of Medicine, Dentistry and Pharmaceutical Sciences, Okayama University, Okayama, Japan.

*To whom correspondence should be addressed:

Takanori Eguchi, DDS, PhD

2-5-1, Shikata-cho, Kita-ku, Okayama city, 700-8525, Japan

Tel: +81-86-235-6662; Fax: +81-86-235-6664

Email: eguchi@okayama-u.ac.jp

**Running title**: PEX domain of MMPs involves cancer metastasis

**Keywords:** nuclear MMP, PEX domain, non-proteolytic MMP, cancer metastasis, tumor stroma.

Number of figures: 7

Number of tables: 2

Number of supplemental items: 3

Number of references: 25

Word count: 5220 (introduction to discussion)

**FUNDING.** This work was supported by JSPS KAKENHI, grant numbers JP17K17895 (to Y.O), JP17K11642 (to T.E.), JP26293067 (to K.K.), JP26670815 (to K.K.), Start-up Grant for Young Scientists at Okayama Univ. (to Y.O.), Molecular Imaging Micro Dose Phase 0 Grant at Okayama Univ. (to Y.O. and K.K.), Gender Equality Grant at Okayama Univ. (to Y.O.), and a Ryobi Teien Memorial Foundation Grant (to T.E.).

**Abbreviations:** PEX, hemopexin-like repeat; MMP, matrix metalloproteinase; RNAi, RNA interference; siRNA, small interfering RNA; HSP, heat shock protein; CTGF, connective tissue growth factor; IHC, Immunohistochemistry.

**Abstract ( < 150 words)**

Members of matrix metalloproteinase (MMP) family promote cancer cell migration, invasion, and metastasis through alteration of the tumor milieu, intracellular signaling pathways, transcription. We examined gene expression signatures of colon adenocarcinoma cell lines with different metastatic potentials and found that rapidly metastatic cells powerfully expressed genes encoding MMP3 and MMP9. The non-proteolytic PEX isoform and proteolytic isoforms of MMPs were significantly expressed in the metastatic cells *in vitro*. Knockdown of MMP3 attenuated cancer cell migration and invasion *in vitro* and lung metastasis *in vivo*. Profound nuclear localization of MMP3 / PEX was found in tumor-stroma marginal area. In contrast, MMP9 was localized in central area of subcutaneous tumors. Overexpression of the PEX isoform of MMP3 promoted proliferation and migration of the rapidly metastatic cells *in vitro*. Taken together, the non-proteolytic PEX isoform of MMPs locating in cell nuclei involves proliferation, migration, and subsequent metastasis of aggressive adenocarcinoma cells.

## INTRODUCTION

Metastasis is a critical phenomenon in cancer. Over time, malignant cancer cells undergo clonal evolution, which promotes their diversity and heterogeneity, as well as therapy resistance [Greaves and Maley, 2012; Kreso and Dick, 2014; Nowell, 1976]. In addition, it has been proposed that highly evolved clones of cancer cells are resistant to selective pressure by the immune, chemo- and radiation therapies. Although previously considered to be mutually exclusive models, it is recently considered that genetic evolution and cancer stem cell models can be harmonized in three related biological fields; tumor genetics, epigenetics and pathways, and microenvironment [Kreso and Dick, 2014]. Matrix metalloproteinases (MMPs) represent the most prominent family of proteinases associated with tumorigenesis and regulators of the tumor microenvironment [Kessenbrock et al., 2013; Kessenbrock et al., 2010]. MMPs have also been reported to be potent biomarkers of tumor progression as well as one of the causal factors that promote multiple processes of tumorigenesis, including oxidative stress-dependent DNA damage and chromosomal instability, epithelial-to-mesenchymal transition (EMT) [Radisky et al., 2005], migration and invasion of cancer cells [Sato H et al., 1994], angiogenesis, and metastasis [Kessenbrock et al., 2013; Kessenbrock et al., 2010; Vandenbroucke and Libert, 2014]. Canonical proteolytic roles for MMPs is to cleave substrate proteins at extracellular space. Proteolysis of extracellular matrix (ECM) and intercellular adhesion molecules by MMPs enable cells to migrate and invade and to release cytokines, chemokines, and growth factors that activate their receptors and intracellular signaling pathways. In addition to those indirect activations of the extracellular factors, MMPs also directly alter activities of growth factors, cytokines, and chemokines by proteolysis. For example, MMPs are able to cleave connective tissue growth factor (CTGF/CCN2) and then release VEGF leading to angiogenesis [Hashimoto et al., 2002]. Another study showed that MMPs and a disintegrin and metalloproteinases cleave

membrane-bound heparin-binding EGF-like growth factor (HB-EGF) and release soluble HB-EGF, which binds to cells and stimulates EGFR/ERBB signaling [Prenzel et al., 1999].

Intracellular and nuclear roles for MMPs have been recently discovered. We showed that MMP3 possesses nuclear localization signals and can translocate into cellular nuclei, in which MMP3 can bind to chromatin proteins and DNA leading to transcriptional regulation of *CTGF/CCN2* gene [Eguchi et al., 2008]. MMP3 is composed of a protease domain, a hinge region, and a C-terminal hemopexin-like repeat (PEX) domain, which is non-proteolytic (see later figure). We recently showed that a PEX isoform of MMP3 activate some members of heat shock protein (HSP) genes [Eguchi et al., 2017], which can contribute to anti-apoptosis and drug resistance. MMP3 can interact with heterochromatin proteins, members of the chromobox protein family that involve transcriptional and chromosomal control [Eguchi et al., 2017; Eguchi et al., 2008; Eguchi et al., 2010]. MMPs also involve oxidative stress, DNA damage, and chromosome instability in cell nuclei. Intranuclear MMP2 and MMP9 activities have been shown to cleave PARP-1 and XRCC1, nuclear matrix proteins, thus promoting oxidative DNA damage and apoptosis in an ischemic injury model [Yang et al., 2010]. MMP3-induced EMT and genomic instability have been shown to be mediated by small GTPase Rac1b and a reactive oxygen species in breast adenocarcinoma and pancreatic cancer [Mehner et al., 2014; Radisky et al., 2005], indicating potent roles for MMPs in proteotoxic and genotoxic stress.

MMPs appear to be appropriate target molecules in treatments of aggressive types of cancers. Although more than 50 MMP inhibitors have been investigated in clinical trials for various cancers, all of those trials failed [Vandenbroucke and Libert, 2014]. However, the involvement of intracellular and non-proteolytic roles for MMPs in cancer have not well-investigated yet.

In the present study, we first investigated gene expression of MMPs correlated with

metastatic phenotype of colon cancer cells. We then assessed nuclear localization of the PEX domain of MMP3 and MMP9 in primary and lung-metastatic tumors and their roles in proliferation, migration, invasion and metastasis of the aggressive cancer cells.

## MATERIALS AND METHODS

**Cells.** Colon26 (also known as colon26), LuM1, and NM11 cells were maintained in RPMI1640 with 10% FBS supplemented with penicillin, streptomycin, and amphotericin B [Hyuga S et al., 1994; Sakata K et al., 1996; Tsuruo et al., 1983].

**Comprehensive gene expression analysis and bioinformatics**. Cells were cultured for 3 days and total RNA was extracted from cultured cells using the AGPC method with Trizol (Molecular Research Center, Cincinnati, OH). Concentration and quality (A260/A280) of total RNA were determined. cDNA was synthesized from 0.1 μg of total RNA using a Low Input Quick Amp Labeling Kit (Agilent Technologies, Santa Clara, CA), then hybridized to probes of a SurePrint G3 Mouse GE 8x60 K v.2 Microarray system (Agilent Technologies, Santa Clara, CA). Gene expression and ratios were analyzed using MeV 4.0 software (http://www.Tm4.org/mev.html). Functional annotation clustering and pathway analysis were performed with LuM1 genes expressed at a 10-fold or higher level as compared to the NM11 and Colon26 cells ($p < 0.05$) using DAVID Bioinformatics Resources 6.8. Relative expression levels in LuM1 or NM11 to the levels in Colon26 were shown in heat maps and bar graphs.

**RNAi**. Cells were transfected with small interfering RNA (siRNA) targeting mRNA of *Mmp3* or *Mmp9* (ON-TARGETplus SMARTpool siRNA; Thermo Fisher Scientific, Rockford, IL), or non-targeting double strand RNA (dsRNA) (siGENOME Control Pool Non-Targeting siRNA) at

a final concentration of 50 nM using DharmaFECT 1 (Thermo Fisher Scientific, Rockford, IL). Cells were cultured for 48 hours before RT-qPCR, Western blot, migration assay, invasion assay and subcutaneous injection and for 72 hours before zymography. For analysis of culture supernatant, cells were cultured for 48 hours in serum-containing medium and subsequently 24 hours in serum-free medium. To examine mRNA levels in tumors, total RNA was extracted from subcutaneous tumors on the day 10 after subcutaneous injection. Lung metastasis assay and immunohistochemistry (IHC) were performed on the day 20 after subcutaneous injection as depicted in Fig. S2A.

**Real-time RT-qPCR**. Total RNA preparation and RT-qPCR was carried out as described previously [Eguchi et al., 2017; Eguchi et al., 2008]. The miRNeasy mini kit (Qiagen) was used with DNase (Qiagen). Total RNA concentration was measured by using a microspectrometer K2800 (Beijing Kaiao, Beijing, China). cDNA synthesis was carried out by using iScript™ cDNA Synthesis Kit (Bio-Rad). Specific primer pairs for *Mmp3, Mmp9, Actb,* and *Gapdh* were used as follows: mMMP3Fw, 5'-ACC AAC CTA TTC CTG GTT GCT GCT and mMMP3Rv, 5'-ATG GAA ACG GGA CAA GTC TGT GGA [Ma et al., 2009]; mMMP9Fw, 5'-CAG CCG ACT TTT GTG GTC TT and mMMP9Rv, 5'-GCT TCT CTC CCA TCA TCT GG [Sousa et al., 2014]; mGapdhFw, 5'-ACC ACA GTC CAT GCC ATC AC and mGapdhRv, 5'-TCC ACC ACC CTG TTG CTG TA [You et al., 2012]; mActb-Fw, 5'-AAC GAG CGG TTC CGA TG and mActb-Rv, 5'-GGA TTC CAT ACC CAA GAA GGA [Sousa et al., 2014]. Realtime PCR was carried out using iQ SYBR Green PCR mixture (Bio-Rad). Relative mRNA levels to *Actb* or *Gapdh* mRNA levels were quantified by the ΔΔCt method using the formula as follows: fold change = $2^{-\Delta\Delta Ct}$. PCR was carried out in triplicate and mean values were calculated with the

mean ± S.D. of biological triplicates.

**Migration and invasion assays**. Migration and invasion assays were performed as previously described [Sakata K et al., 1996]. Uncoated and Matrigel-coated culture systems (Becton Dickinson) were used for *in vitro* migration and invasion assays, respectively. For knockdown experiments, cells were transfected with siRNA and then cultured for 48 hours before re-seeding to upper chambers. Cells were seeded at concentrations of $5 \times 10^4$ per an upper chamber of a Transwell® 24-well (Corning) for the migration assay and of $2.5 \times 10^4$ per an upper chamber of a Transwell® 24-well for the invasion assay. Cells transfected with PEX-overexpressing or control plasmids were seeded at concentrations of $5 \times 10^4$ per an upper chamber of a Transwell® 24-well for the migration assay and of $1.6 \times 10^4$ per an upper chamber of a Transwell® 24-well for invasion assay. Cells that migrated or invaded through the pores to the lower surface of filter were fixed, stained using Diff-Quick stain (Sysmex) and counted after 6 hours of migration period or 19 hours of invasion period for knockdown experiments, and after 0, 12 and 24 hours for comparison of different cell lines. To evaluate the effects of the transfection, percentages of migrated and invaded cells relative to the control were calculated.

**Cell proliferation.** Cells were transfected with siRNA or plasmid DNA and then seeded at a concentration of $3.8 \times 10^3$ cells / well in a 96-well plate on the day 2 after transfection. Number of cells at 1 to 4 days post-transfection period were counted by using Countess automated cell counter (Invitrogen). Floid® cell imaging station (ThermoFisher Scientific) was used for photomicrography.

**Allogeneic transplantation**. All animal experiments were performed according to the

guidelines for care and use of laboratory animals approved by Okayama University and the Japanese Pharmacological Society. Subcutaneous allogeneic transplantation was performed as previously described [Sakata K et al., 1996], with 5.0 x $10^5$ cells transplanted subcutaneously into a side abdominal wall of each 6 to 7-week-old BALB/c mouse. Twenty days after transplantation, subcutaneous tumors and lungs were resected, then fixed with Bouin's fluid. Nodules larger than 0.5-mm-diameter were counted.

**Casein and gelatin zymography.** For zymography of non-transfected cells, cells were inoculated at a concentration of 2 x $10^6$ cells into 60-mm culture dishes in 4 ml of RPMI1640 containing 10% FBS and cultured overnight, then incubated in serum-free medium for 24 hours. Cell culture supernatants were concentrated 20 times using an Amicon filtration tube (for MW 10,000). Cells were washed with PBS, collected using a cell scraper, and lysed in RIPA buffer containing a protease inhibitor cocktail (Sigma-Aldrich, St Louis, MO), then further lysed by homogenization (25-gauge needle, 10 strokes) and incubated for 30 minutes on ice. Lysates were centrifuged at 12,000 x *g* for 20 minutes to remove debris and supernatants were used as cell lysates. Twenty microgram of cell lysates or 4 μg of cell culture supernatants were mixed with an SDS sample buffer and $CaCl_2$ (5 mM final concentration), then applied to 10% acrylamide gel containing copolymerized 0.1% gelatin (Cosmo Bio, Tokyo, Japan). For zymography with knockdown experiments, cells were cultured in 6-well plates. At 48 hours after transfection, medium was replaced with serum-free medium and cells were cultured for 24 hours, then the supernatants were ultra-filtrated and concentrated as described above. Following a protein assay, 9 μg of the >10-kDa cell culture supernatant was mixed with a 2x sample buffer (10 μl) and 1 μl of 50 mM $CaCl_2$, then separated on 10% acrylamide gels containing copolymerized 0.1% gelatin or 0.5% casein (CosmoBio, Tokyo, Japan). The gels were washed

with wash buffer for 30 minutes at RT and incubated for 40 hours in enzyme reaction buffer at 37˚C. Coomassie Brilliant Blue staining was performed and photographs of the gels were obtained, then quantitative densitometric analysis was performed using Image J.

**Western blotting analysis.** Cells were seeded into 6-well plates and transfected with siRNA using the procedure described above, then lysed in RIPA buffer as described above. Next, 30-μg protein samples were separated by SDS-PAGE on 10% poly-acrylamide gels and transferred to PVDF membranes. The membranes were blocked in Tris-buffered saline containing 0.05% Tween 20, 2.5% skim milk, and 2.5% BSA for 30 minutes at room temperature (RT). Each membrane was incubated with the primary antibody (1/1000) overnight at 4˚C and subsequently incubated with horseradish peroxidase (HRP)-conjugate secondary antibodies against anti-rabbit IgG (GE Healthcare) (1/2000) for 1 hour at RT in the blocking solution. Blots were visualized with a Clarity Western ECL Substrate (Bio-Rad).

**Antibodies.** Rabbit monoclonal anti-PEX domain MMP3 antibody (EP1186Y, ab52915) and a rabbit polyclonal anti-MMP9 antibody (ab38898, full-length protein corresponding to mouse MMP9 was immunized) were purchased from Abcam.

**Immunohistochemistry**. Excised tumor tissues were immediately fixed in Bouin's fluid, then dehydrated by passage through an ethanol series and embedded in paraffin. Samples were cut into 4-μm serial sections, which were then placed onto saline-coated slides. Deparaffinized sections were treated with methanol containing 0.3% $H_2O_2$ for 30 minutes to block endogenous peroxidase activity. Sections were then autoclave heated in 10 mM of citrate buffer solution (pH 6.0) for 10 minutes at 120˚C for antigen retrieval. Blocking was performed using a Dako Chem

Mate Envision Kit/HRP. Sections were incubated with the anti-MMP3 antibody (ab52915; 1/100) overnight at 4˚C and subsequently with a secondary antibody against anti-rabbit IgG HRP-conjugated (K400211-2, EnVision+ Single Reagents, Dako) for 1 hour at 4˚C. IHC reaction products were visualized by use of a diaminobenzidine chromogen substrate. Samples were then counterstained with hematoxylin and observed with a BZ-X700 (Keyence, Osaka, Japan). For a negative control, sections were incubated with omission of the primary antibody under the same protocol.

**Immunofluorescence and confocal microscopy.** For immunofluorescence staining, excised tumor tissues were immediately fixed in Bouin's fluid, then dehydrated by passage through an ethanol series and embedded in paraffin. Samples were cut into 4-μm serial sections, which were then placed onto saline-coated slides. Blocking was performed using a Dako Chem Mate Envision Kit. Sections were incubated with the anti-MMP3 antibody (ab52915; 1/100) and the anti-MMP9 antibody (ab38838; 1/500) overnight at 4˚C and subsequently with a secondary antibody against anti-rabbit IgG (ab150076; 1/5000) for 1 hour at 4˚C. For a negative control, sections were incubated with omission of the primary antibody under the same protocol. After three washes with TBS, the mounting and DNA staining were performed by using ProLong gold AntiFade reagents with 4_,6-diamino-2-phenylindole (DAPI) (Molecular Probes, Invitrogen). Fluorescence images were taken using a confocal laser scanning microscopy LSM780 (Carl Zeiss). We defined four areas of a subcutaneous tumor as follows: the stromal as an outside of the tumor margin, the marginal as an area 0 to 30 μm apart from the tumor margin, the interior as an area 30 to 80 μm apart from the outside of the marginal area. According to this definition, MMP3/9 and/or DAPI positive cells in each area were counted using Image J. The nuclear MMP positive rate was calculated as follows: MMP3/9 and DAPI double positive nuclei per

DAPI positive nuclei.

**Plasmid constructs and transfection.** pFlag3-PEX-myc and pFlag3-myc were described previously [Eguchi et al., 2018]. These plasmid constructs were transfected using NEPA21 electroporator (NEPA Gene, Ichikawa, Japan). To optimize transfection condition and efficiency for LuM1, ten different conditions of electroporation was tested. An optimized electroporation condition with 150V and 5 ms pulse twice was then used for plasmid transfection.

**Statistical analysis.** Statistical significance was calculated using Microsoft Excel. Three or more mean values were compared using one way analysis of variance (ANOVA), while comparisons of 2 were done with an unpaired Student's *t*-test. $p < 0.05$ was considered to indicate statistical significance.

## RESULTS

### Gene expression signatures and gene screening of high- and low-metastatic cancer cell lines.

We first examined gene expression signatures of colon adenocarcinoma cell lines with different metastatic potentials in high-metastatic LuM1, low-metastatic NM11 and the parental Colon26 cells. To characterize these cell types with different invasive and metastatic potentials at gene expression levels, microarray analysis was carried out. (Raw data was submitted to the Gene Expression Omnibus (GEO) database repository; accession ID: GSE97166; Colon26, GSM2553008; LuM1, GSM2553009; NM11, GSM2553010.) Among the 62,976 genes tested, 479 genes were strongly expressed at a greater than 10-fold higher level in the metastatic LuM1 as compared to the low-metastatic lines (Fig. 1A; Fig. S1). Functional annotation clustering and

pathway analysis then revealed that the gene expression signature of LuM1 involved particular biological events in the extracellular microenvironment, cell adhesion, immunology, and protein interactions (Table 1, 2). In addition, functional classification of those LuM1-specific genes indicated that these 104 genes specifically expressed in LuM1 involved cancer cell invasion, EMT, and metastasis (Fig. 1B). These results indicated that more than a hundred metastasis-related genes involved metastatic, invasive and transforming potential of the LuM1 cells. Among the 104 metastasis-related genes expressed specifically in LuM1 cells, several members of *Mmp* gene family, were profoundly expressed. We therefore examined *Mmp* expression signatures in the LuM1, NM11, and Colon26 cells. Of note, the gene expression level of *Mmp3* in the metastatic LuM1 was the highest among all *Mmp* gene family members and higher than that in Colon26 and NM11 (2400.9-fold and 4.6-fold, respectively, Fig. 1C, D; Fig. S1C) . *Mmp9* was also expressed in the LuM1 at a high level, as compared to the low-metastatic Colon26 and NM11 (512.1-fold and 237.8-fold, respectively, Fig.1D).

These results indicate that *Mmp3* and *Mmp9* were profoundly co-expressed in the metastatic adenocarcinoma cells.

**Targeted knockdown of MMP3 attenuates proliferation, migration and invasion of the metastatic adenocarcinoma cells.**

We next examined migration and invasion activities of metastatic LuM1 cells and low-metastatic NM11 cells, as well as of their parental low-metastatic adenocarcinoma cell line Colon26. LuM1 showed the highest levels of migration and invasion as compared to the other low metastatic lines (Fig. 2A-C). We then examined siRNA-mediated knockdown of MMP3 and MMP9. Both MMP3 and MMP9 at mRNA levels were specifically and efficiently reduced by their targeted siRNA (Fig. 2 D, E). (Later figures show knockdown at protein levels). Yet the

MMP3 siRNA increased the MMP9 mRNA level (Fig. 2E) and, in contrast, the MMP9 siRNA increased the MMP3 mRNA level (Fig. 2D), suggesting compensatory expression system of these essential MMPs. (Some mutual compensation was also seen in Western blotting and zymography as shown in later figures).

We next examined roles of MMP3 and MMP9 in regard to proliferation of LuM1 cells. The MMP3 siRNA (50 nM) tended to attenuate proliferation of the LuM1 cells whereas the MMP9 siRNA (50 nM) and MMP9/MMP3 siRNA mixture (each 25nM) did not (Fig. 2F, Fig. S2B). The MMP3 siRNA and MMP3/MMP9 siRNA attenuated the migration of LuM1 cells to 46.9% and 51.3%, respectively, of the level of the control (Fig. 2G), and attenuated invasion to 71.0% and 59.7%, respectively (Fig. 2H). The MMP9 siRNA attenuated migration of the LuM1 to 69.6%, which was a lesser effect as compared to MMP3-targeting, and did not alter invasion (Fig. 2G, H).

These results indicate that MMP3 is a key protein in the proliferation, migration, and invasion of the aggressive adenocarcinoma cells.

**Targeted reduction of MMP3 and MMP9 attenuates primary and lung-metastatic tumorigenesis of the aggressive adenocarcinoma cells.**

We next examined whether knockdown of MMP3 and MMP9 could alter primary tumor development and lung metastasis of the LuM1 cells in the allogeneic transplantation experiments. As pilot studies, we tested sustainability of siRNA-mediated knockdown as follows. The RNAi effect on MMP9 was sustained for 96 hours after transfection to LuM1 cells, as shown by gelatin zymography (Fig. S2C). Of note, RNAi effects on *Mmp3* and *Mmp9* at mRNA levels were sustained in tumors *in vivo* even at day 10 after subcutaneous injection (Fig. S2D). Using this knockdown system, we examined whether MMP3- and MMP9-targeting

siRNA alter tumor development and metastasis. The weights of primary tumors were reduced by the MMP3 siRNA and the MMP9 siRNA on day 20 after the transplantation, as compared to the control (Fig. 3A, B).

The number of metastatic nodules in lungs were significantly reduced by the MMP3 siRNA, the MMP9 siRNA and the MMP3/MMP9 siRNA, as compared to the control (Fig. 3C, D). The weights of lungs bearing the metastatic nodules were significantly reduced by the MMP3 siRNA, the MMP9 siRNA and the MMP3/MMP9 siRNA, as compared to the control (Fig. 3E).

These results suggest that targeted knockdown of MMP3 and MMP9 reduce primary tumor development and subsequent metastasis of aggressive adenocarcinoma cells.

**The intracellular non-proteolytic PEX domain of MMP3 and the short MMP9 were expressed in the metastatic adenocarcinoma cells.**

We next examined expression and proteolytic activities of several isoforms of the MMPs produced from the metastatic LuM1 cells, and examined siRNA-mediated knockdown of these *in vitro*, based on that MMPs had been historically demonstrated as extracellular proteases, whereas non-proteolytic and intracellular roles for MMPs have been recently shown [Eguchi et al., 2017; Eguchi et al., 2008]. Therefore, prior to detection, we organized structures of MMP3 and MMP9 (Fig. 4A, B). We examined isoforms of MMP3 produced in the LuM1 cells at by performing siRNA-mediated knockdown and subsequent Western blotting analysis and zymography. (Full images of Western blot and zymography were shown in supplemental Fig. S3.) The anti-PEX domain MMP3 antibody detected both full-length 54-kDa (arrow) and short 25-kDa PEX domain (arrowhead) of MMP3 (Fig. 4C). The MMP9 siRNA increased the PEX of MMP3 and decreased full-length MMP3 (Fig. 4C, compare lane 1 and lane 3), indicating

crosstalk between MMP3 and MMP9. We next examined MMP3 proteolytic activity in the culture supernatant of the LuM1 cells in casein zymography. The 54-kDa and 100-kDa proteinases lysed casein, and these were thought to be proteolytic MMP3 monomer and dimer, respectively (Fig. 4 D, control si). The proteolytic MMP3 monomer was reduced by the MMP3 siRNA (arrow), whereas the proteolytic putative MMP3 dimer was not reduced by the MMP3 siRNA, but reduced by MMP3/MMP9 siRNA (arrowhead) (Fig. 4D), indicating crosstalk between MMP3 and MMP9. As expected, the non-proteolytic 25-kDa PEX domain was not detected in the casein zymography.

We next examined isoforms of MMP9 produced from the LuM1 cells. Intracellular gelatinase activities of approx. 90-kDa and 250-kDa proteinases were significantly found in both lysate (Fig. 4E) and culture supernatant (Fig. 4F) of the metastatic LuM1 cells, but at much lower levels in the other low-metastatic cell lines. The 90-kDa gelatinase was thought to be MMP9 and the 250-kDa gelatinase was thought to be oligomers of MMP9.

We next examined knockdown of the intracellular and extracellular MMP9 produced by LuM1 cells. The anti-MMP9 antibody detected full-length (approx. 90-kDa, arrow), processed forms (64- and 67-kDa, arrowhead), and putative oligomer (250-kDa, asterisk) of MMP9 in the lysate of LuM1 cells (Fig. 4G). Gelatinase activities of the 90-kDa MMP9 in the cell culture supernatant of LuM1 cells treated with the MMP9 siRNA was lower than that treated with the control siRNA or the MMP3 siRNA (Fig. 4H).

These results indicate that the non-proteolytic PEX domain of MMP3 and the short MMP9 were intracellularly produced in the metastatic adenocarcinoma cells. The siRNAs targeting MMP3/9 successfully reduced proteolytic and non-proteolytic intracellular and extracellular isoforms of MMPs.

**Expression and nuclear localization of MMP3 in primary tumors and in metastatic lungs in allogeneic transplants.**

MMP3 was initially found as the first member of stromelysin, which lyse ECMs in stroma. Later studies have shown intranuclear localization and roles of MMP3 [Eguchi et al., 2017; Eguchi et al., 2008]. In the present study, *Mmp3* was notably expressed in the metastatic LuM1 *in vitro*. We next examined expression and subtumoral and subcellular localization of MMP3 in primary tumors and in lungs with metastatic tumors in an allogeneic transplant model. As it have been shown that the PEX domain of MMP3 has an essential role in transcriptional regulation [Eguchi et al., 2017], we used an anti-PEX MMP3 antibody in immunohistochemistry. MMP3 was expressed at relatively high levels at marginal zone of tumor parenchyma (P) to stroma (S) in primary tumors, but at lower levels in central area of the parenchyma (Fig. 5A, B). Notably, intranuclear MMP3 was found in both marginal parenchymal cells (arrowheads) and stromal cancer-associated fibroblast (CAF)-like cells (arrow) (Fig. 5C).

We next examined subtumoral and subcellular localization of MMP3 in the metastatic lungs in the same model. MMP3-positive cells were found throughout the metastatic tumor nodules and in pulmonary alveolar locations (Fig. 5E). MMP3 was found inside nuclei (arrow) and the nuclear margins (arrowhead) of cells with nuclear polyploidy in metastatic tumors in the lung (Fig. 5F).

These results indicate that extra- and intracellular MMP3 involve CAF-related invasion, nuclear polyploidy, and metastasis of the aggressive adenocarcinoma cells.

**Nuclear PEX domain / MMP3 localized in tumor-stroma marginal area and MMP9 localized in central area of tumors.**

To more precisely investigate the nuclear localization of MMP3/9 in tumors, we next used immunofluorescence and confocal laser scanning microscopy and examined nuclear MMP3/9 positive rate in each tumor area. We defined four areas of a tumor as follows: central (Fig. 6A, left), interior, marginal and stromal areas (Fig. 6A, right). The rate of cells with nuclear MMP3 was most significant in the stromal area (17.6 %) and next in the tumor marginal area (9.4 %) as compared to those in the interior (0.80 %) and central areas (0.73%) with the lower rate (Fig. 6B - D). On the other hand, nuclear MMP9 positive cells were found notably in the central area (2.5 %) as compared to the other areas (Fig. 6B, D).

We next assessed localization of MMP3 and MMP9 in a lung lesion with metastatic tumors. Tumor cells with nuclear MMP3/9 appeared to scatter throughout the metastatic cancer nodule in the lung and in pulmonary alveolar locations (Fig. 6E), consisting with IHC data shown in Fig. 5.

Of note, DNA stained with DAPI appeared to be dot-like condensation in cell nuclei in both primary and metastatic tumors (Fig. 6C-E), indicating chromosomal condensation involving gene regulation. MMP3 and MMP9 appeared to co-localize with DNA (Fig. 6C-E, arrows), suggesting DNA-binding and gene regulation. MMP3 and MMP9 appeared to localize out of nuclei- cytoplasm or extracellular region as well.

These results indicate that nuclear PEX domain / MMP3 localized in primary tumor-stroma marginal area and lung-metastatic tumor nodules. Nuclear MMP9 localized in central area of primary tumors and in lung-metastatic tumor nodules.

**Overexpression of the PEX-domain promotes proliferation and migration of the metastatic cancer cells.**

We next asked whether the non-proteolytic PEX domain could alter proliferation, migration,

and invasion of the aggressively metastatic cancer cells. Overexpression of the PEX of MMP3 significantly increased proliferation of LuM1 cells (Fig. 7A). Of note, overexpression of the PEX increased migration of LuM1 cells to 204% level of the control (Fig. 7B). Overexpression of the PEX tended to increase invasion of LuM1 cells to 127.1% level of the control (Fig. 7C), suggesting that protease activities of MMPs might promote invasion rather than the non-proteolytic PEX.

These results indicate that the PEX-domain has key roles in abilities of proliferation and migration of the metastatic adenocarcinoma cells.

**DISCUSSION**

MMP family members are consist of secretory types (collagenases, gelatinases, stromelysins) and membrane types (MT-MMPs) and have crucial roles in the progression of diseases, including cancer, arthritis, and periodontitis. Most metalloproteinase inhibitors had been designed and, indeed, to block catalytic pockets that possess a zinc ion and proteinase activity. However, any metalloproteinase inhibitor has been approved for clinical application. Recent studies, including the present study, have shown intracellular and non-proteolytic roles for MMPs in arthritis and cancer [Eguchi et al., 2017; Eguchi et al., 2008; Eguchi et al., 2010]. In addition to in an arthritis model and in a chondrosarcoma-derived cell line [Eguchi et al., 2008], nuclear MMP3 was significantly found in primary tumors and in metastatic sites in allogeneic transplant model of the aggressive adenocarcinoma cells (Fig. 5, 6). Both the PEX isoform and full-length MMP3 were significantly found in the metastatic LuM1 cells (Fig. 4). The siRNA targeting MMP3 reduced both 25-kDa PEX isoform and 54-kD full-length MMP3 (Fig. 4C) and simultaneously attenuated proliferation and migration of the aggressive adenocarcinoma cells (Fig. 2 F, G). On the other hand, overexpression of the PEX isoform promoted proliferation and

migration of the LuM1 cells (Fig. 7). Therefore, the PEX isoform and domain are responsible for MMP-driven cell proliferation, migration and subsequent metastasis of the aggressive adenocarcinoma cells.

MMP3 and MMP9 colocalized with DNA in subcutaneous tumors *in vivo* (Fig. 6). These data indicated potential roles for MMP3 and MMP9 in gene regulation in primary and metastatic tumors. We showed that MMP3 localized in cell nuclei in stroma-tumor marginal cells in subcutaneous tumors (Fig. 5B, 5C, 6B, 6C), suggesting that MMP3 involves potential tumor-stromal interaction such as induction of CAFs, migration, invasion and tumor angiogenesis, tumor-immunology interaction through the stroma. In contrast, MMP9 was localized in central area of subcutaneous tumors (Fig. 6 B, D). Central area of tumors are often necrotic and/or hypoxic where hypoxia-inducible transcription factor (HIF1) controls transcription of target genes, including MMP genes [Kondo, 2002] and stem cell genes [Eguchi et al., 2018; Keith et al., 2011; Keith and Simon, 2007; Semenza, 2016]. We previously showed that MMPs and CTGF/CCN2 were inducible upon hypoxia through distinctive mechanisms [Kondo, 2002]. MMP9 is one of key proteins induced by HIF1 in tumors whereas CTGF could be increased through mRNA stabilization [Kondo, 2002]. Thus, HIF1, MMP9, and CTGF can be co-increased at central area of tumors and the induced MMP9 and CTGF can promote tumor angiogenesis [Kondo, 2002]. CTGF may be increased by transcriptional role for MMP9 in central area of tumors (Fig. 6D), in addition to the role for MMP3 in transcription [Eguchi et al., 2017; Eguchi et al., 2008] . Indeed, mRNA levels of CTGF were altered in tumors *in vivo* upon knockdown of MMP3 and MMP9 (data not shown). Thus, we are further investigating mechanisms underlying MMPs regulation of CTGF and HSPs that may mediate tumor progression and metastasis.

In addition to the intracellular and non-catalytic roles for MMP3 as shown above,

intracellular and non-catalytic MMP9 was suggested in the present study. The approx. 60-kDa MMP9 isoforms were significantly detected in the lysate of the metastatic LuM1 cells (Fig. 4G). However, any intracellular proteolytic activity of the 60-kDa MMP9 was not detected in the lysate of LuM1 cells, even though the gelatinase activities of 90-kDa and 250-kDa MMP9 were found (Fig. 4F) and extracellular proteinase activity of 60-kDa MMP9 was detected in the cell culture supernatant (Fig. 4H). Thus, the intracellular 60-kDa MMP9 does not possess any proteolytic activity or some intracellular factors such as DNA/chromatin might mask the proteinase domain.

Of note, the non-proteolytic MMPs cannot be directly targeted by metalloproteinase inhibitors that block proteolytic pockets. Moreover, the intranuclear MMPs might be difficult to be accessed by small molecule drugs, which can be excreted from cancer cells, and are much more difficult by molecularly targeted antibody drugs, which are too large to enter into cells and nuclei. The siRNA-mediated knockdown tested in the present study significantly and sustainably reduced intracellular and extracellular, non-catalytic and catalytic MMPs (Fig. 4, S3). These efficient knockdown of various isoforms of MMPs might involve their efficient effects to attenuate migration, invasion and metastasis. The RNAi approaches are able to target mRNAs that fundamentally encode proteins that are post-translationally modified, processed and localized to specific regions. Thus, the RNAi approaches might be more fundamentally effective in disease therapies.

It was recently reported that MMP3 functions in a coordinated manner with a chemokine, IL-8/CXCL8, expressed in melanoma via direct regulation by NFAT1, thus promoting tumor progression and metastasis [Shoshan et al., 2016]. Another recent study found that interleukin-regulatory transcription factor 8 (IRF-8) directly repressed the *Mmp3* gene in relatively mild mammary tumor cells, whereas loss of IRF-8 in coordination with gain in *Mmp3*

expression promoted tumor progression and metastasis [Banik et al., 2015.]. These studies were done using xenotransplantation of human cancer cells into immunodeficient mice. We consider that the present protocol of allogeneic transplantation into an immunologically genetically relatively normal host will be useful for further studies of tumor microenvironment and immunology.

Thus, intracellular and non-proteolytic MMPs have crucial roles in cancer progression. The versatile RNAi approach is able to reduce intracellular and extracellular, non-proteolytic and proteolytic MMPs at once and thus appears to be significantly effective to attenuate various aspects of cancer progression, including proliferation, migration and invasion of cancer cells, tumor development and metastasis.

**ACKNOWLEDGEMENTS.** This paper is dedicated to the memory of one of the coauthors, Professor Ken-ichi Kozaki, who passed away on May 29, 2016. The authors thank Toshifumi Fujiwara, Kisho Ono, Tomoko Yamamoto and Kazumi Ohyama for their technical assistance and useful discussion.

**CONFLICTS OF INTEREST**. The authors have no competing financial interests to declare.

**REFERENCES**

Banik D, Netherby CS, Bogner PN, Abrams SI. 2015. MMP3-mediated tumor progression is controlled transcriptionally by a novel IRF8-MMP3 interaction. Oncotarget 6:15164-79.

Eguchi T, Calderwood SK, Takigawa M, Kubota S, Kozaki KI. 2017. Intracellular MMP3 Promotes HSP Gene Expression in Collaboration With Chromobox Proteins. J Cell Biochem 118:43-51.

Eguchi T, Kubota S, Kawata K, Mukudai Y, Uehara J, Ohgawara T, Ibaragi S, Sasaki A,

Kuboki T, Takigawa M. 2008. Novel transcription-factor-like function of human matrix metalloproteinase 3 regulating the CTGF/CCN2 gene. Mol Cell Biol 28:2391-413.

Eguchi T, Kubota S, Kawata K., Mukudai Y., Uehara J., Ohgawara T., Ibaragi S, Sasaki A., Kuboki T, Takigawa M. 2010. Novel Transcriptional Regulation of CCN2/CTGF by Nuclear Translocation of MMP3. Dordrecht, Nertherlands: Springer. p 255-264.

Eguchi T, Sogawa C, Okusha Y, Uchibe K, Iinuma R, Ono K, Nakano K, Murakami J, Itoh M, Arai K, Fujiwara T, Namba Y, Murata Y, Shimomura M, Okamura H, Takigawa M, Nakatsura T, Kozaki K, Okamoto K, Calderwood S. 2018. Organoids with Cancer Stem Cell-like Properties Secrete Exosomes and HSP90 in a 3D NanoEnvironment. PLOS ONE 13:e0191109.

Greaves M, Maley CC. 2012. Clonal evolution in cancer. Nature 481:306-13.

Hashimoto G, Inoki I, Fujii Y, Aoki T, Ikeda E, Okada Y. 2002. Matrix metalloproteinases cleave connective tissue growth factor and reactivate angiogenic activity of vascular endothelial growth factor 165. J Biol Chem 277:36288-95.

Hyuga S, Nishikawa Y, Sakata K, Tanaka H, Yamagata S, Sugita K, Saga S, Matsuyama M, Shimizu S. 1994. Autocrine factor enhancing the secretion of M(r) 95,000 gelatinase (matrix metalloproteinase 9) in serum-free medium conditioned with murine metastatic colon carcinoma cells. Cancer Res 54:3611-6.

Keith B, Johnson RS, Simon MC. 2011. HIF1alpha and HIF2alpha: sibling rivalry in hypoxic tumour growth and progression. Nat Rev Cancer 12:9-22.

Keith B, Simon MC. 2007. Hypoxia-inducible factors, stem cells, and cancer. Cell 129:465-72.

Kessenbrock K, Dijkgraaf GJ, Lawson DA, Littlepage LE, Shahi P, Pieper U, Werb Z. 2013. A role for matrix metalloproteinases in regulating mammary stem cell function via the Wnt signaling pathway. Cell Stem Cell 13:300-13.

Kessenbrock K, Plaks V, Werb Z. 2010. Matrix metalloproteinases: regulators of the tumor microenvironment. Cell 141:52-67.

Kondo S, Kubota, S., Shimo, T., Nishida, T., Yosimichi, G., Eguchi, T., ... & Takigawa, M. . 2002. Connective tissue growth factor increased by hypoxia may initiate angiogenesis in collaboration with matrix metalloproteinases. Carcinogenesis.

Kreso A, Dick JE. 2014. Evolution of the cancer stem cell model. Cell Stem Cell 14:275-91.

Ma O, Cai WW, Zender L, Dayaram T, Shen J, Herron AJ, Lowe SW, Man TK, Lau CC, Donehower LA. 2009. MMP13, Birc2 (cIAP1), and Birc3 (cIAP2), amplified on chromosome 9, collaborate with p53 deficiency in mouse osteosarcoma progression. Cancer Res 69:2559-67.

Mehner C, Miller E, Khauv D, Nassar A, Oberg AL, Bamlet WR, Zhang L, Waldmann J, Radisky ES, Crawford HC, Radisky DC. 2014. Tumor cell-derived MMP3 orchestrates Rac1b and tissue alterations that promote pancreatic adenocarcinoma. Mol Cancer Res 12:1430-9.

Nowell PC. 1976. The clonal evolution of tumor cell populations. Science 194:23-8.

Prenzel N, Zwick E, Daub H, Leserer M, Abraham R, Wallasch C, Ullrich A. 1999. EGF receptor transactivation by G-protein-coupled receptors requires metalloproteinase cleavage of proHB-EGF. Nature 402:884-888.

Radisky DC, Levy DD, Littlepage LE, Liu H, Nelson CM, Fata JE, Leake D, Godden EL, Albertson DG, Nieto MA, Werb Z, Bissell MJ. 2005. Rac1b and reactive oxygen species mediate MMP-3-induced EMT and genomic instability. Nature 436:123-7.

Sakata K, Kozaki K, Iida K, Tanaka R, Yamagata S, Utsumi KR, Saga S, Shimizu S, Matsuyama M. 1996. Establishment and characterization of high- and low-lung-metastatic cell lines derived from murine colon adenocarcinoma 26 tumor line. Jpn J Cancer Res (Cancer Sci) 87:78-85.

Sato H, Takino T, Okada Y, Cao J, Shinagawa A, Yamamoto E, Seiki M. 1994. A matrix metalloproteinase expressed on the surface of invasive tumour cells. Nature 370:61-5.

Semenza GL. 2016. The hypoxic tumor microenvironment: A driving force for breast cancer progression. Biochim Biophys Acta 1863:382-91.

Shoshan E, Braeuer RR, Kamiya T, Mobley AK, Huang L, Vasquez ME, Velazquez-Torres G, Chakravarti N, Ivan C, Prieto V, Villares GJ, Bar-Eli M. 2016. NFAT1 Directly Regulates IL8 and MMP3 to Promote Melanoma Tumor Growth and Metastasis. Cancer Res 76:3145-55.

Sousa NG, Cardoso CR, Silva JS, Kuga MC, Tanomaru-Filho M, Faria G. 2014. Association of matrix metalloproteinase inducer (EMMPRIN) with the expression of matrix metalloproteinases-1, -2 and -9 during periapical lesion development. Arch Oral Biol 59:944-53.

Tsuruo T, Yamori T, Naganuma K, Tsukagoshi S, Sakurai Y. 1983. Characterization of Metastatic Clones Derived from a Metastatic Variant of Mouse Colon Adenocarcinoma 26. Cancer Res 43:5437-5442.

Vandenbroucke RE, Libert C. 2014. Is there new hope for therapeutic matrix metalloproteinase inhibition? Nat Rev Drug Discov 13:904-27.

Yang Y, Candelario-Jalil E, Thompson JF, Cuadrado E, Estrada EY, Rosell A, Montaner J, Rosenberg GA. 2010. Increased intranuclear matrix metalloproteinase activity in neurons interferes with oxidative DNA repair in focal cerebral ischemia. Journal of Neurochemistry 112:134-149.

You S, Avidan O, Tariq A, Ahluwalia I, Stark PC, Kublin CL, Zoukhri D. 2012. Role of epithelial-mesenchymal transition in repair of the lacrimal gland after experimentally induced injury. Invest Ophthalmol Vis Sci 53:126-35.



## FIGURE LEGENDS

**Figure 1. Transcriptome analysis, gene screening, *Mmp* genes expressed in colon cancer cells with different metastatic potential.** (A) Flow chart of gene screening. Microarray screened 62976 genes. The 479 genes were expressed at more than 10-fold higher level in LuM1 as compared to NM11 and Colon26 cells. (B) Venn diagram extracted 104 genes involved in invasion, EMT, and metastasis. (C) Heat map analysis of *Mmp* gene family. The gene expression levels relative to the levels in Colon26 were shown. (D) Expression levels of *Mmp* genes in LuM1, NM11 and Colon26 cells. The gene expression level of *Mmp3* in LuM1 was the highest among all *Mmp* gene family members, as well as compared to that in NM11 and Colon26 cells.

**Figure 2. The roles of MMP3 and MMP9 in proliferation, migration, and invasion of the metastatic adenocarcinoma cells.** (A) Differential *in vitro* migration activities. Migrated cells per well was shown. The migration activity of LuM1 was higher than that of NM11 and Colon26 cells.

*$p$ < 0.05 as compared with Colon26 (one way ANOVA). n = 3. (B) Differential *in vitro* invasion activities. *$p$ < 0.05 as compared with Colon26 (one way ANOVA). n = 3. (C) Staining of invaded cells. Diff-Quick staining was carried out after invasion assay. Scale bars: 200 μm. (D) The mRNA levels of MMP3 in the LuM1 cells transfected with siRNA. Relative mRNA levels normalized to *Gapdh* mRNA levels were shown. *$p$ < 0.05 as compared with control si group. †$p$ < 0.05 as compared with Mmp9 si group (one way ANOVA). n = 3. (E) The mRNA levels of MMP9 in the LuM1 cells transfected with siRNA. Relative mRNA levels normalized to *Gapdh* mRNA levels were shown. *$p$ < 0.05 as compared with control si group. †$p$ < 0.05 as compared with MMP3 si group (one way ANOVA). n = 3. (F) Growth curves of LuM1 cells transfected with MMP-targeting or control siRNA. (G, H) *In vitro* migration (G) and invasion (H) activities altered by MMP3 and/or MMP9 knockdown. Upper panels, quantified migration (G) and invasion (H) activities of LuM1 cells transfected with siRNA-targeting MMP3, MMP9, MMP3/MMP9 or the control dsRNA. n = 5. *$p$ < 0.05 as compared to the control si group (one way ANOVA). Lower panels, migrated (G) and invaded (H) cells stained with Diff-Quick. Scale bars: 200 μm. Control si group, n = 5; MMP3 si group, n = 5; MMP9 si group, n = 5; MMP3/9 si group, n = 6. *$p$ < 0.05 as compared to the control si group. †$p$ < 0.05 as compared to the MMP9 si group (one way ANOVA). Lower panel, Invaded cells stained with Diff-Quick. Scale bars: 200 μm.

**Figure 3. Targeting MMP3 and MMP9 attenuated tumor development and metastasis of the aggressive colon cancer cells.** LuM1 cells transfected with siRNA targeting MMP3 and/or MMP9 or non-targeting dsRNA were subcutaneously injected to abdominal walls in mice. The primary tumors and the metastatic tumors in lungs were analyzed 20 days post-injection period. (A) Representative images of mice bearing subcutaneous primary tumors. (B) Weights of

subcutaneous primary tumors. (C) Representative images of lungs with metastatic tumor nodules. (D) Numbers of metastatic tumor nodules in lungs. (E) Weights of lungs with metastatic tumor nodules. (C-E) Control si group, n = 5; MMP3 si group, n = 5; MMP9 si group, n = 5; MMP3/9 si group, n = 6. *$p < 0.05$, as compared to the control si group (one way ANOVA).

**Figure 4. Knockdown of non-proteolytic and proteolytic, intracellular and extracellular MMP3 and MMP9.** (A) Schematic structures of murine MMP3. The structures of protease domain-containing 54-kDa MMP3 and non-proteolytic 25-kDa PEX domain of MMP3 are shown. The anti-PEX MMP3 antibody EP1186Y recognizes the epitope 450 to 477 position, which both the 54-kDa MMP3 and the 25-kDa PEX isoform contain. PG, peptide glycan binding domain. PEX, hemopexin-like repeat. Asterisks are positions of nuclear localization signals. (B) Schematic structures of approx. 92-95-kDa MMP9 and 64- and 67-kDa MMP9. Fn, fibronectin type II domain. PT, PT repeat composed on the tetrapeptide xPTx. (C) Western blot showing intracellular isoforms of MMP3 in the LuM1 cells and those knockdown. An arrow indicates full-length MMP3 (54-kDa). An arrowhead indicates the intracellular 25-kDa PEX isoform of MMP3. WCL, whole cell lysate. (D) Casein zymography of extracellular isoforms of MMP3 and those knockdown in the LuM1 cells. An arrow indicates full-length MMP3 (54-kDa). An arrowhead indicates proteolytic MMP3 monomer or dimer. M, molecular weight maker. (E) Intracellular gelatinase activities in the LuM1 cells. The WCLs prepared from LuM1, Colon26 and NM11 were examined in zymography. Gelatinase activities at approx. 90-kDa (arrow) and 250-kDa (asterisk) were seen. (F) Extracellular gelatinase activities in the culture supernatant of the LuM1 cells. Gelatinase activities at approx. 90-kDa (arrow) and 250-kDa (asterisk) were seen. (G) Western blotting analysis of intracellular isoforms of MMP9 in the

lysate of LuM1 cells and those knockdown. An arrow indicates approx. 90-kDa MMP9. An arrowhead indicates intracellular short MMP9 (64- and 67-kDa). An asterisk indicates putative intracellular oligomer of MMP9. (H) Gelatin zymography of extracellular MMP9 and those knockdown in the LuM1 cells. Gelatinase activities were seen at approx. 90-kDa (arrow, the major band), 60-kDa (arrowhead), and 250-kDa (asterisk). M, molecular weight maker.

**Figure 5. The subtumoral and subcellular localization of the PEX / MMP3 in primary tumors and in metastatic tumors in lungs.** LuM1 cells were subcutaneously injected into abdominal walls in a mouse. A developed subcutaneous primary tumor (A-C) and a lung lesion (D-F) with metastatic tumor nodules were prepared at day 20 after the injection and then immunohistochemistry of the PEX / MMP3 was performed. (A) A whole tumor. Scale bar: 500 μm. (B) A magnified view of the box shown in A. Scale bar: 50 μm. (C) A magnified view of the box shown in B. Scale bar: 10 μm. An arrow indicates MMP3 immunostained in a cancer-associated fibroblast (CAF)-like cell. Arrowheads indicate nuclear localization of MMP3. (D) A whole lung with metastasis. Scale bar: 500 μm. (E) A magnified view of the box shown in D. Scale bar: 50 μm. (F) A magnified view of the box shown in E. Scale bar: 10 μm. An arrow indicates MMP3 accumulated in the nucleus. An arrowhead indicates MMP3 localization to the nuclear margin.

**Figure 6. The nuclear PEX / MMP3 found in tumor-stroma marginal area and nuclear MMP9 in tumor central area.** For immunostaining, an anti-PEX MMP3 antibody and anti-MMP9 full-length were used. (A) The scheme of definition of the central area (shown in the left photomicrograph), interior, marginal and stromal areas (shown in the right photomicrograph) of a tumor. Scale bars, 500 μm (left) and 10 μm (right). The area in the

rectangle in the left image was shown with a high power magnification in the right image. (B) The positive rate of MMP3 and MMP9 in the nuclei in individual area. n = random 3 fields. *$p$ < 0.05 as compared to the nuclear MMP3 positive rate in the stromal area. (C, D) Confocal microscopy of subtumoral and subcellular localization of MMP3 (C) and MMP9 (D). Red, MMP3 or MMP9. Blue, DNA stained with DAPI. Arrows indicate the MMP3 or MMP9 localization in the nuclei. Scale bars, 10 μm (C) and 20 μm (D). (E) Confocal microscopy of subcellular localization of MMP3/9 in the lung lesion with metastatic cancer cells. Arrows indicate MMP3 (left) and MMP9 (right) positive region in the nuclei. Scale bars, 5 μm.

**Figure 7. The potent roles of the PEX-domain in proliferation and migration of the metastatic cancer cells.** (A) Growth curves of the metastatic LuM1 cells transfected with pFlag3-PEX-myc or the control vector. *$p$ < 0.05 as compared with control vector. (B) *In vitro* migration activities altered by overexpression of the PEX domain. Upper panels, staining of the migrated cells. Scale bars: 200 μm. Lower panel, ratio of migrated cells upon overexpression of the PEX domain or the control vector. n = 3. *$p$ < 0.05 as compared with control vector. (C) *In vitro* invasion activities. Upper panels, staining of the invaded cells. Scale bars: 100 μm, Lower panel, ratio of the invaded cells upon overexpression of the PEX domain or the control vector. n = 3.

## SUPPORTING INFORMATION LEGENDS

**Figure S1. Expression signatures of *Mmp* gene family in rapidly metastatic LuM1, slowly metastatic NM11 and the parental Colon26 cells.** (A) Differential migration activities of the tested cells after the treatment with trypsin or EDTA. LuM1 cells treated with trypsin migrated more than other cell lines or EDTA-treated LuM1 cells. EDTA is a chelator for metal. MMPs

coordinate a zinc ion at their activity pockets. EDTA chelates zinc ions coordinated in proteins, including MMPs. The chelation of zinc ion in MMPs may alter their structures and functions. Trypsin cleaves and alters cell surface proteins, possibly including receptor-bound MMPs and MT-MMPs. Scale bars: 200 μm. (B) Quality check of the total RNA by agarose gel electrophoresis. The quality of RNA samples were confirmed before microarray and RT-qPCR analysis. (C) Heat map showing relative expression levels of all *Mmp* gene family members. The gene expression level of *Mmp3* in LuM1 was the highest among all *Mmp* gene family members, as well as compared to that in NM11 and Colon26 cells.

**Figure S2. Targeted knockdown of MMP3 and/or MMP9.** (A) A flowchart of knockdown studies. Cells were cultured for 48 hours after transfection of siRNA. We then performed RT-qPCR (Fig. 2D, E), Western blotting analysis (Fig. 4C, G), migration assay (Fig. 2G), invasion assay (Fig. 2H), and subcutaneous injection (Fig. 3). Cells transfected with siRNA were cultured for 48, 72 or 96 hours for zymography while the media were replaced to serum-free media 24 hours prior to harvest of culture supernatant. To analyze mRNA levels in tumors *in vivo*, total RNA was extracted from subcutaneous tumors on the day 10 after subcutaneous injection. Lung metastasis assay and IHC were performed on the day 20 after subcutaneous injection. (B) Representative photomicrographs of LuM1 cells transfected with siRNAs. Scale bars: 100 μm. (C) Gelatin zymography to examine sustainability of RNAi effect. LuM1 cells were transfected with siRNA targeting Mmp9 or non-silencing control dsRNA. Cell culture supernatants (5 ml) were collected at 48, 72, and 96 hours after transfection, then concentrated to a 1/20 volume. Protein samples (13.2 μg) were subjected to SDS-PAGE for gelatin zymography (upper panel). The #1 and #2 indicate biological duplicates. The intensities of the bands were quantified by using ImageJ and shown in the graph (lower panel). (D) *In vivo*

gene expression levels of *Mmp3* in the MMP3-knockdown tumor (upper) and the levels of *Mmp9* in the MMP9-knockdown tumor (lower). Total RNA was prepared from the tumor on the day 10 after the subcutaneous injection of siRNA-transfected LuM1 cells and qRT-PCR was performed. Relative mRNA levels normalized to *Actb* mRNA levels were shown.

**Figure S3. Full images of Western blot and zymography shown in Fig 6.** (A) Western blotting analysis of intracellular isoforms of MMP3 in the LuM1 cells and those knockdown. (B) Casein zymography of extracellular isoforms of MMP3 and those knockdown in the LuM1 cells. (C) Intracellular gelatinase activities in the LuM1 cells. (D) Extracellular gelatinase activities in the culture supernatant of the LuM1 cells. (E) Western blotting analysis of intracellular isoforms of MMP9 in the lysate of LuM1 cells and those knockdown. (F) Gelatin zymography of extracellular MMP9 and those knockdown in the LuM1 cells.

**Table 1. Functional annotation clustering**.

| Annotation Cluster 1 | Enrichment Score: 2.49 | P-value |
|---|---|---|
| GO:0044421 | extracellular region part | 0.0010483 |
| GO:0005576 | extracellular region | 0.0050501 |
| GO:0005615 | extracellular space | 0.0064459 |
| Annotation Cluster 2 | Enrichment Score: 2.11 | P-value |
| GO:0007155 | cell adhesion | 0.0046972 |
| GO:0022610 | biological adhesion | 0.0047962 |
| GO:0016337 | cell-cell adhesion | 0.0213548 |
| Annotation Cluster 3 | Enrichment Score: 1.90 | P-value |
| GO:0006954 | inflammatory response | 0.00592 |
| GO:0006952 | defense response | 0.0092881 |
| GO:0009611 | response to wounding | 0.0107201 |
| GO:0002252 | immune effector process | 0.0416591 |
| Annotation Cluster 4 | Enrichment Score: 1.83 | P-value |
| GO:0030246 | carbohydrate binding | 4.37E-04 |
| GO:0030247 | polysaccharide binding | 0.0119368 |
| GO:0001871 | pattern binding | 0.0119368 |
| GO:0005539 | glycosaminoglycan binding | 0.0228992 |
| GO:0008201 | heparin binding | 0.0477234 |

Genes expressed at a 10-fold greater level in LuM1 as compared to those in NM11 and Colon26 cells were analyzed.

**Table 2. Ranking of altered pathways in LuM1 as compared to NM11 and Colon26 cells.**

| Category | Term | P-value |
|---|---|---|
| KEGG_PATHWAY | mmu04060:Cytokine-cytokine receptor interaction | 0.0202 |
| KEGG_PATHWAY | mmu04062:Chemokine signaling pathway | 0.0253 |
| KEGG_PATHWAY | mmu04142:Lysosome | 0.0283 |
| KEGG_PATHWAY | mmu04020:Calcium signaling pathway | 0.0325 |

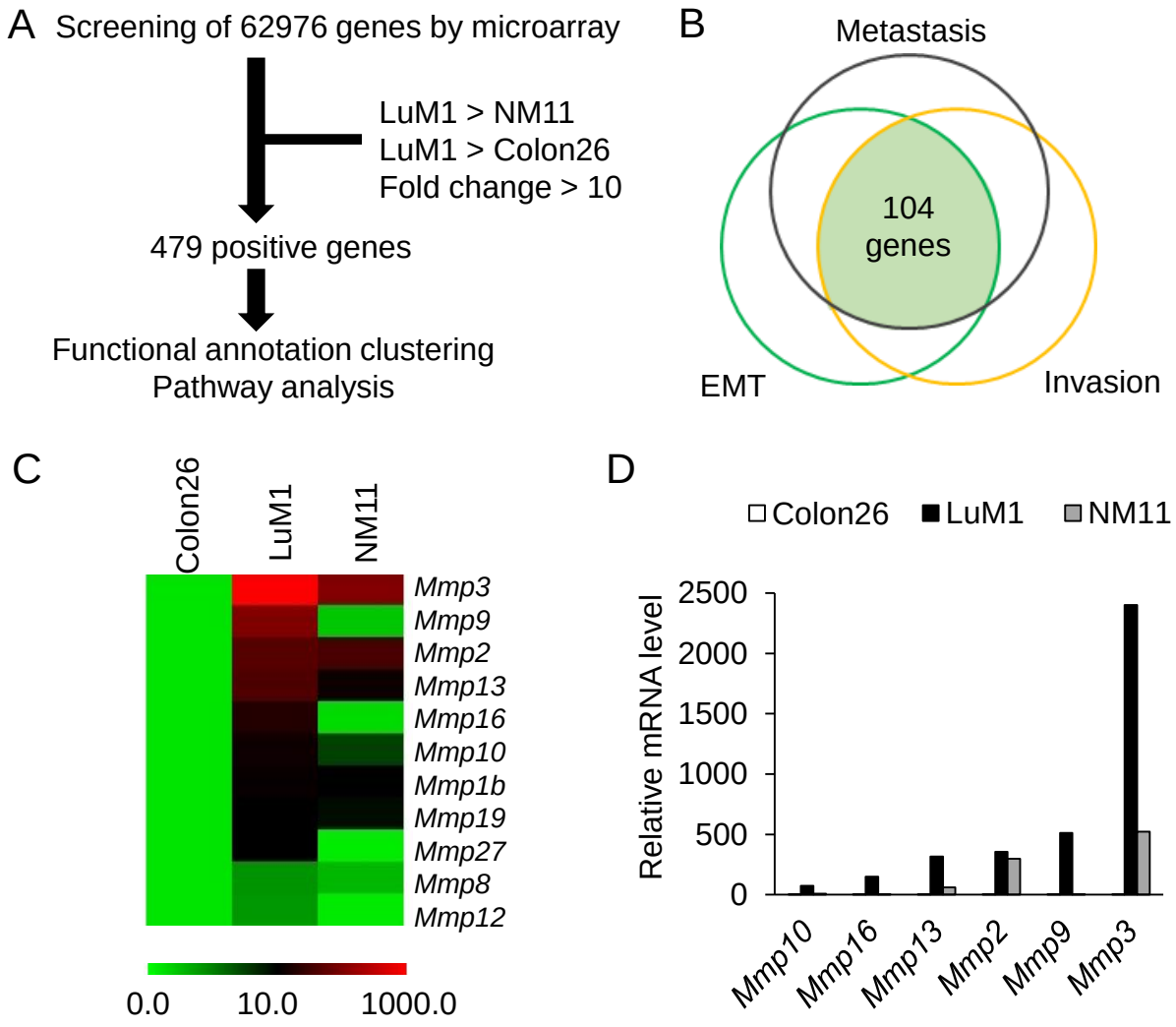
A
Screening of 62976 genes by microarray
LuM1 > NM11
LuM1 > Colon26
Fold change > 10
479 positive genes
Functional annotation clustering
Pathway analysis
B
Metastasis
104
genes
EMT
Invasion
C
Colon26
LuM1
NM11
Mmp3
Mmp9
Mmp2
Mmp13
Mmp16
Mmp10
Mmp1b
Mmp19
Mmp27
Mmp8
Mmp12
0.0
10.0
1000.0
D
Colon26
LuM1
NM11
Relative mRNA level
2500
2000
1500
1000
500
0
Mmp10
Mmp16
Mmp13
Mmp2
Mmp9
Mmp3

Fig. 1

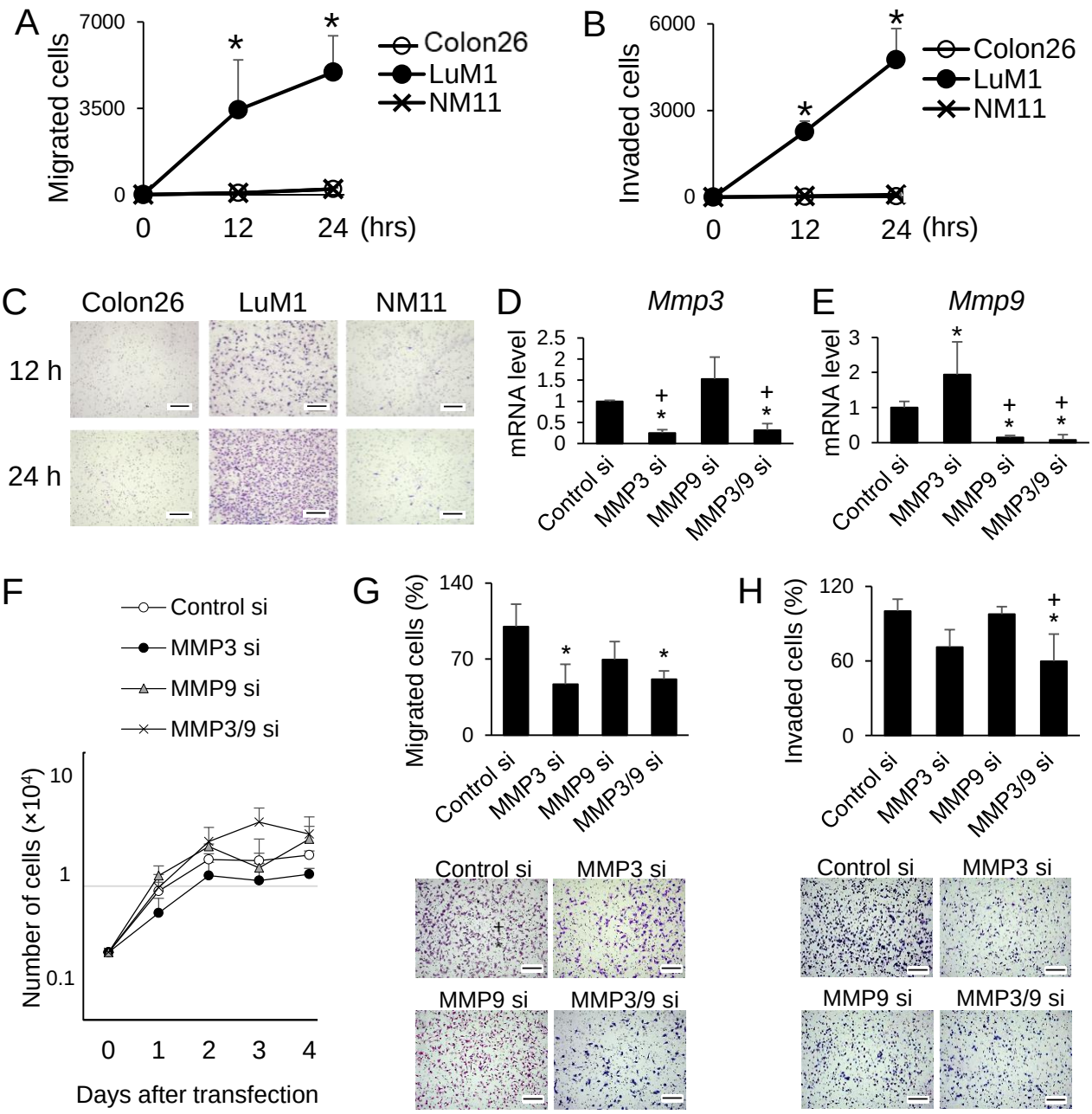
A
Migrated cells
7000
3500
0
0
12
24 (hrs)
Colon26
LuM1
NM11
B
Invaded cells
6000
3000
0
0
12
24 (hrs)
Colon26
LuM1
NM11
C
Colon26
LuM1
NM11
12 h
24 h
D
Mmp3
mRNA level
2.5
2
1.5
1
0.5
0
Control si
MMP3 si
MMP9 si
MMP3/9 si
E
Mmp9
mRNA level
3
2
1
0
Control si
MMP3 si
MMP9 si
MMP3/9 si
F
Control si
MMP3 si
MMP9 si
MMP3/9 si
Number of cells (×10⁴)
10
1
0.1
0
1
2
3
4
Days after transfection
G
Migrated cells (%)
140
70
0
Control si
MMP3 si
MMP9 si
MMP3/9 si
Control si
MMP3 si
MMP9 si
MMP3/9 si
H
Invaded cells (%)
120
60
0
Control si
MMP3 si
MMP9 si
MMP3/9 si
Control si
MMP3 si
MMP9 si
MMP3/9 si



Fig. 2

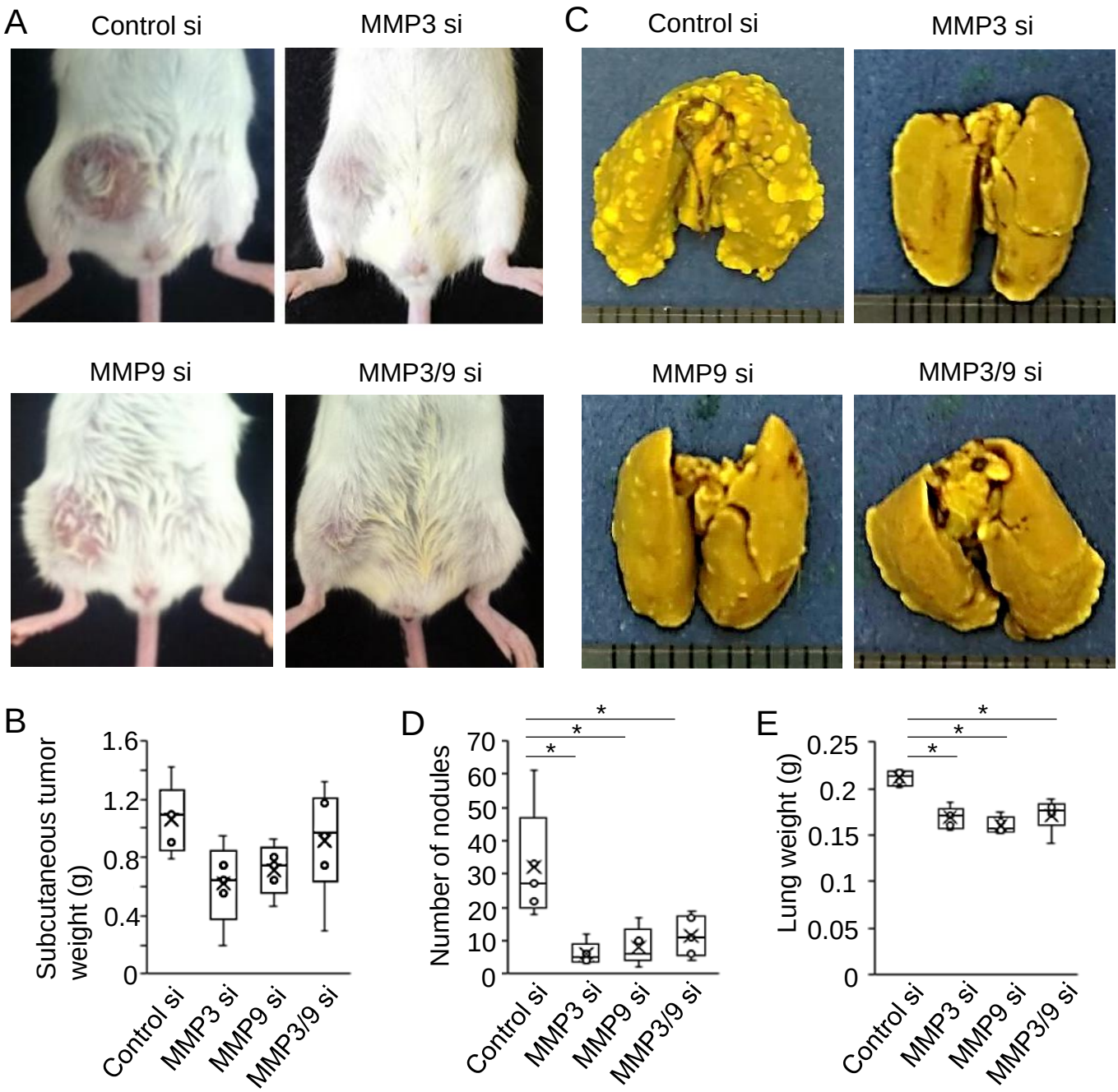
A
Control si
MMP3 si
MMP9 si
MMP3/9 si
C
Control si
MMP3 si
MMP9 si
MMP3/9 si
B
Subcutaneous tumor weight (g)
1.6
1.2
0.8
0.4
0
Control si
MMP3 si
MMP9 si
MMP3/9 si
D
Number of nodules
70
60
50
40
30
20
10
0
*
*
*
Control si
MMP3 si
MMP9 si
MMP3/9 si
E
Lung weight (g)
0.25
0.2
0.15
0.1
0.05
0
*
*
*
Control si
MMP3 si
MMP9 si
MMP3/9 si

Fig. 3

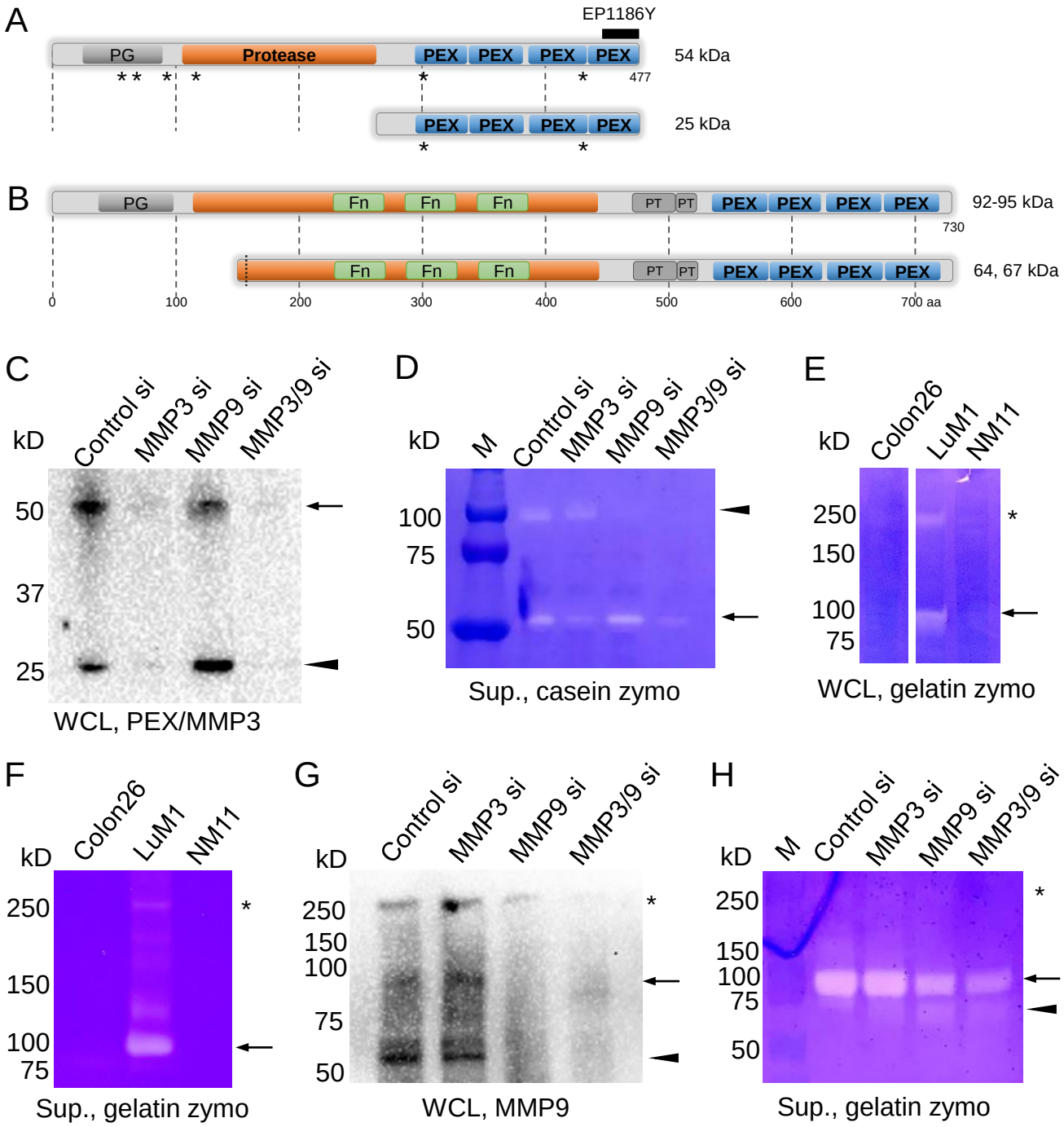
A
EP1186Y
PG
Protease
PEX
PEX
PEX
PEX
54 kDa
477
PEX
PEX
PEX
PEX
25 kDa
B
PG
Fn
Fn
Fn
PT
PT
PEX
PEX
PEX
PEX
92-95 kDa
730
Fn
Fn
Fn
PT
PT
PEX
PEX
PEX
PEX
64, 67 kDa
0
100
200
300
400
500
600
700 aa
C
kD
Control si
MMP3 si
MMP9 si
MMP3/9 si
50
37
25
WCL, PEX/MMP3
D
kD
M
Control si
MMP3 si
MMP9 si
MMP3/9 si
100
75
50
Sup., casein zymo
E
kD
Colon26
LuM1
NM11
250
150
100
75
*
WCL, gelatin zymo
F
kD
Colon26
LuM1
NM11
250
150
100
75
*
Sup., gelatin zymo
G
kD
Control si
MMP3 si
MMP9 si
MMP3/9 si
250
150
100
75
50
*
WCL, MMP9
H
kD
M
Control si
MMP3 si
MMP9 si
MMP3/9 si
250
150
100
75
50
*
Sup., gelatin zymo

Fig. 4

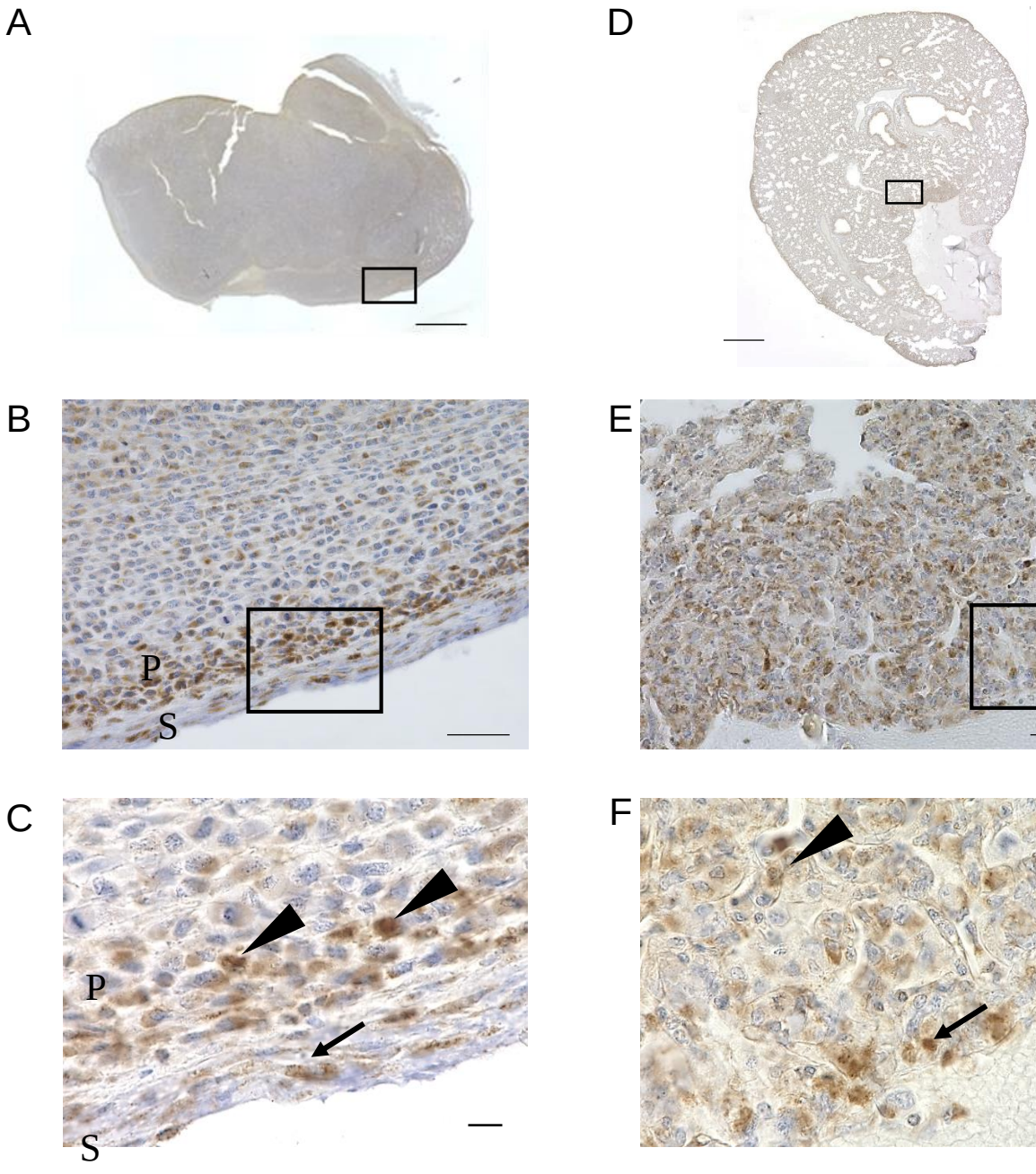


Fig. 5

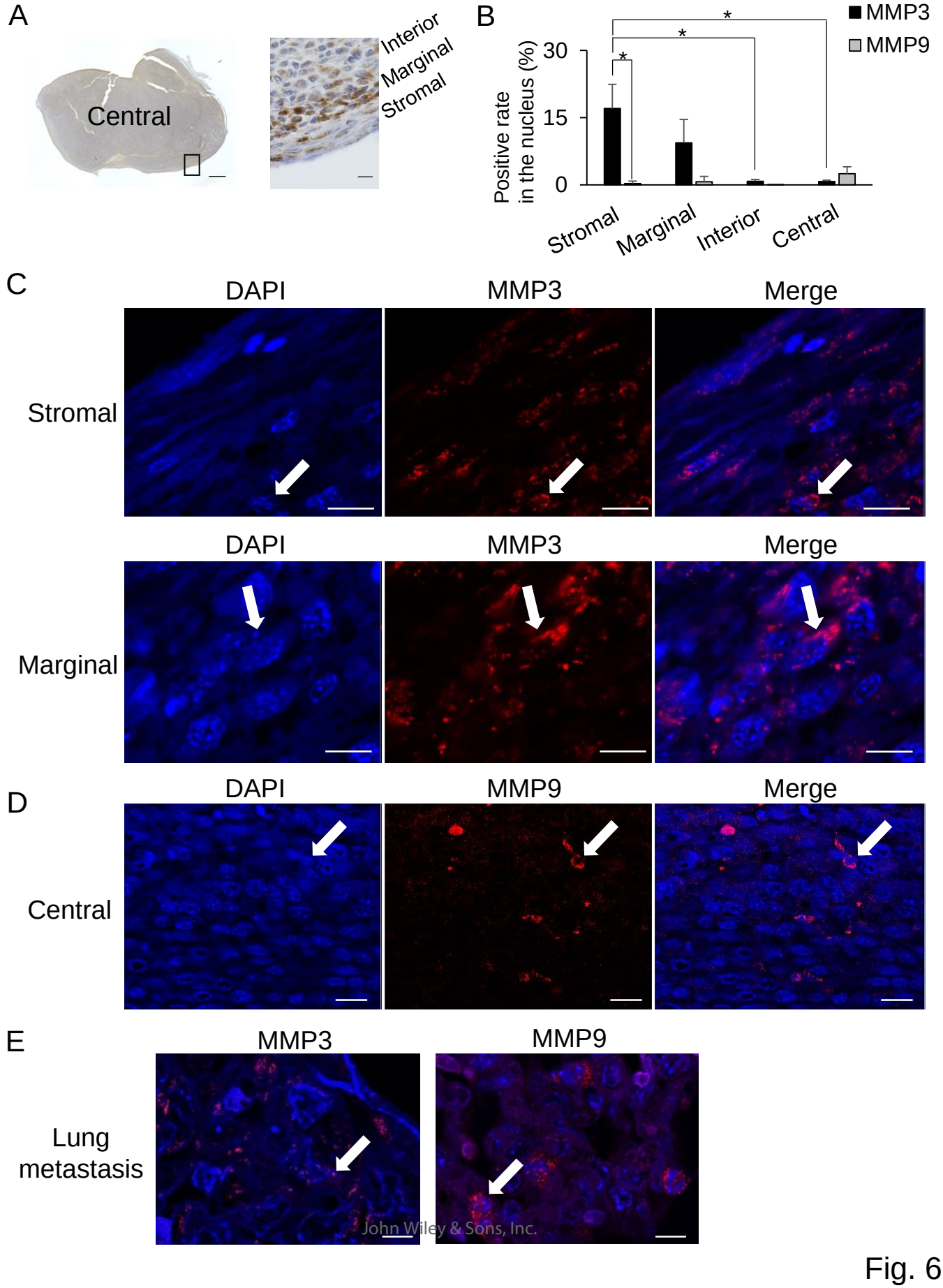




Fig. 6

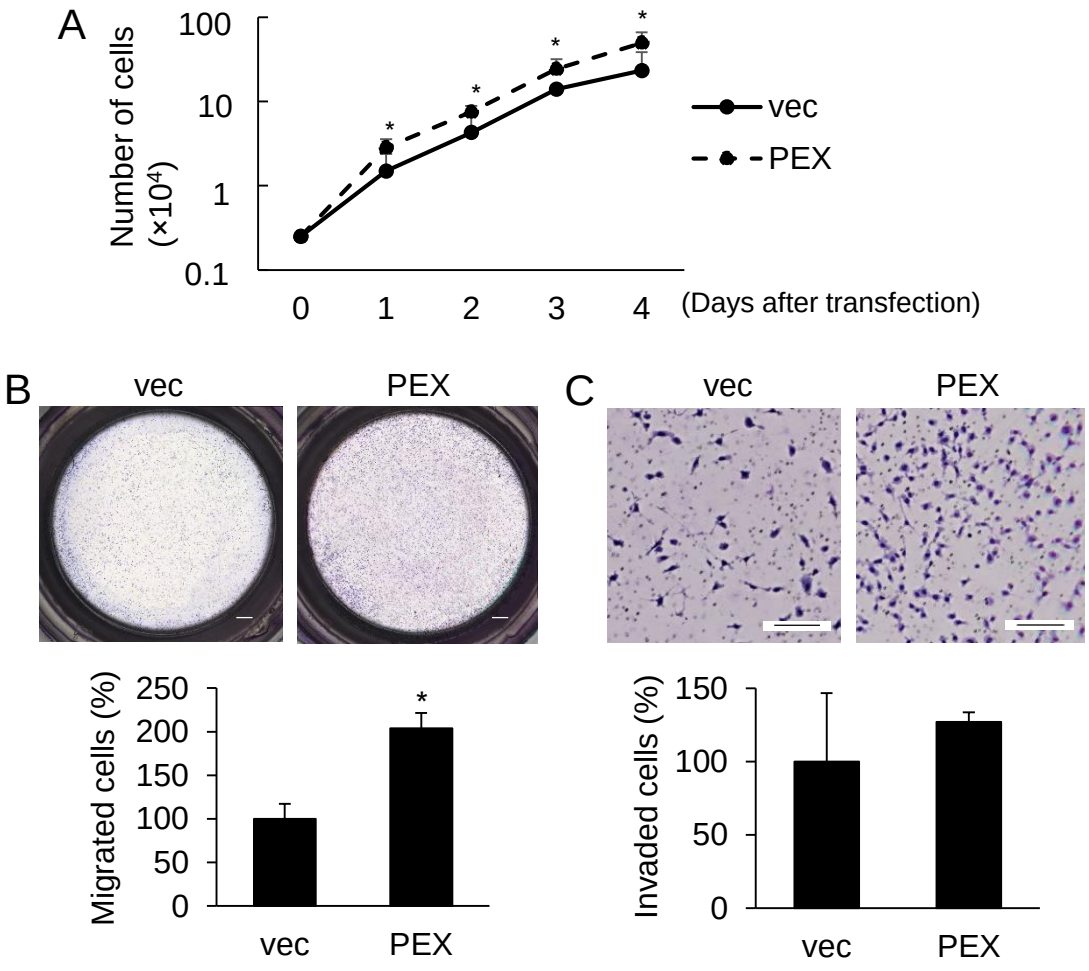
A
Number of cells
(×10⁴)
100
10
1
0.1
0
1
2
3
4
(Days after transfection)
vec
PEX
*
B
vec
PEX
Migrated cells (%)
250
200
150
100
50
0
C
vec
PEX
Invaded cells (%)
150
100
50
0

Fig. 7

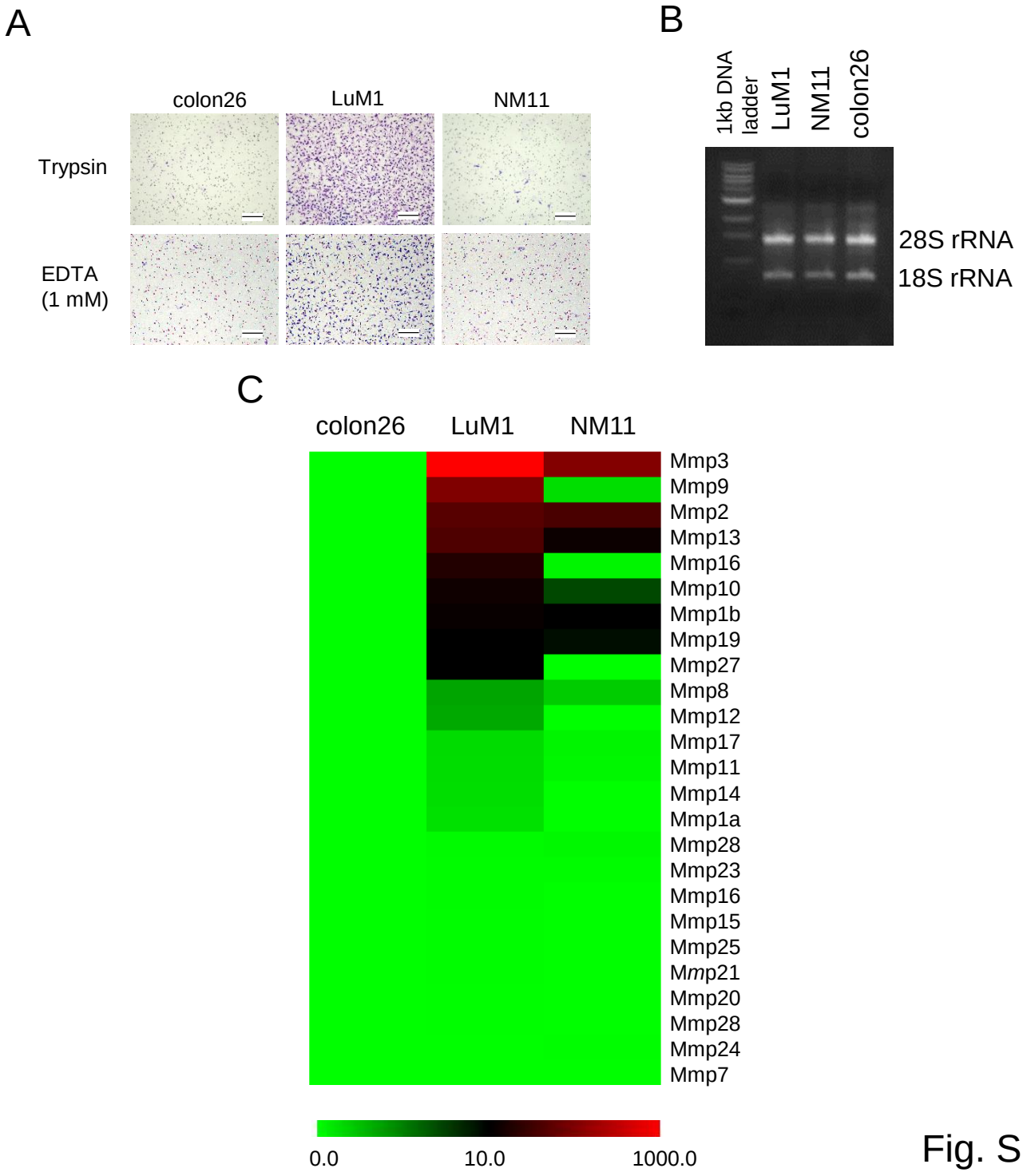
A
colon26
LuM1
NM11
Trypsin
EDTA
(1 mM)
B
1kb DNA ladder
LuM1
NM11
colon26
28S rRNA
18S rRNA
C
colon26
LuM1
NM11
Mmp3
Mmp9
Mmp2
Mmp13
Mmp16
Mmp10
Mmp1b
Mmp19
Mmp27
Mmp8
Mmp12
Mmp17
Mmp11
Mmp14
Mmp1a
Mmp28
Mmp23
Mmp16
Mmp15
Mmp25
Mmp21
Mmp20
Mmp28
Mmp24
Mmp7
0.0
10.0
1000.0

Fig. S1

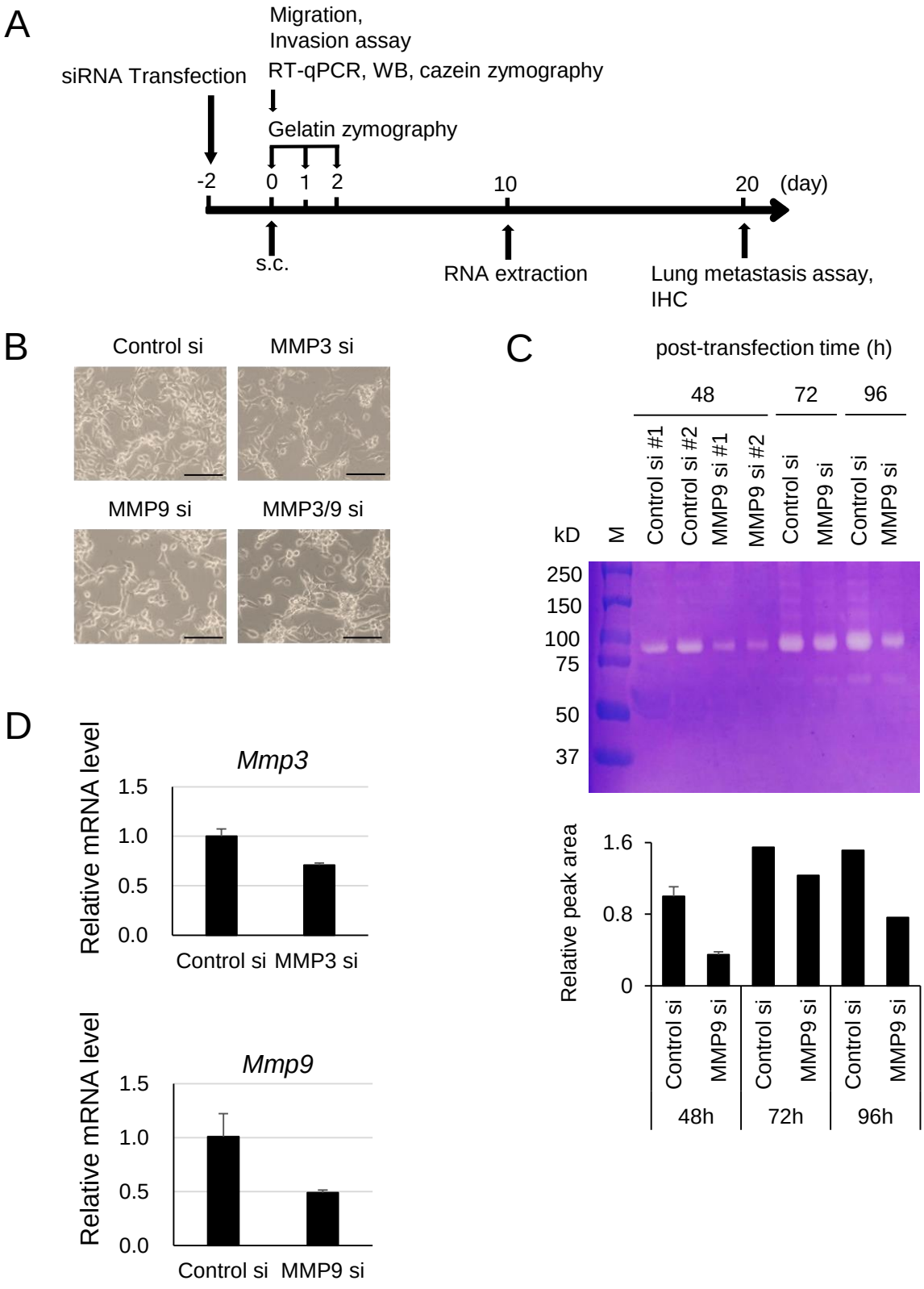
A
Migration,
Invasion assay
siRNA Transfection
RT-qPCR, WB, cazein zymography
Gelatin zymography
-2
0
1
2
10
20
(day)
s.c.
RNA extraction
Lung metastasis assay,
IHC
B
Control si
MMP3 si
MMP9 si
MMP3/9 si
C
post-transfection time (h)
48
72
96
Control si #1
Control si #2
MMP9 si #1
MMP9 si #2
Control si
MMP9 si
Control si
MMP9 si
kD
M
250
150
100
75
50
37
Relative peak area
1.6
0.8
0
Control si
MMP9 si
Control si
MMP9 si
Control si
MMP9 si
48h
72h
96h
D
Mmp3
Relative mRNA level
1.5
1.0
0.5
0.0
Control si
MMP3 si
Mmp9
Relative mRNA level
1.5
1.0
0.5
0.0
Control si
MMP9 si

Fig. S2

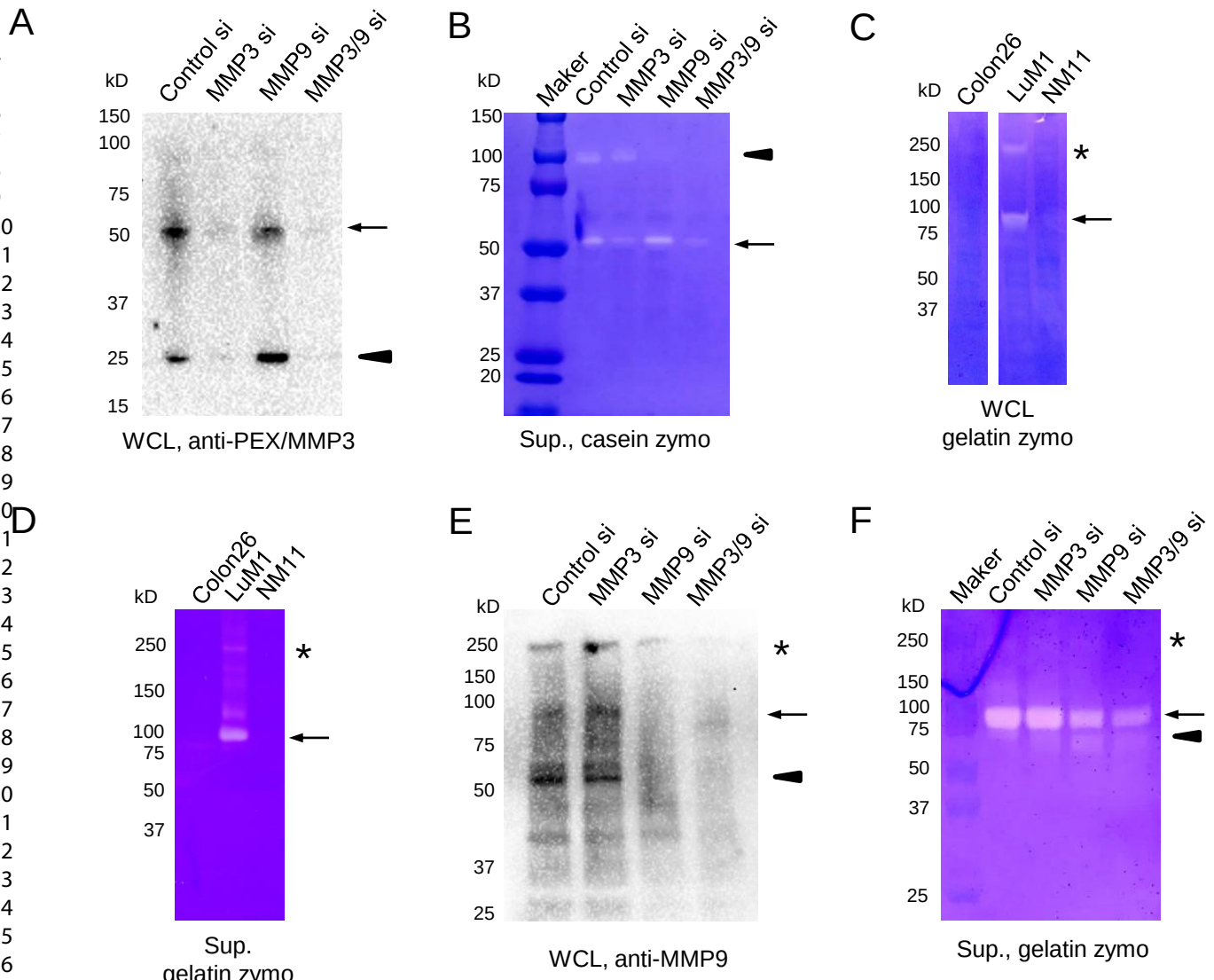
A
Control si
MMP3 si
MMP9 si
MMP3/9 si
kD
150
100
75
50
37
25
15
WCL, anti-PEX/MMP3
B
Maker
Control si
MMP3 si
MMP9 si
MMP3/9 si
kD
150
100
75
50
37
25
20
Sup., casein zymo
C
Colon26
LuM1
NM11
kD
250
150
100
75
50
37
*
WCL
gelatin zymo
D
Colon26
LuM1
NM11
kD
250
150
100
75
50
37
*
Sup.
gelatin zymo
E
Control si
MMP3 si
MMP9 si
MMP3/9 si
kD
250
150
100
75
50
37
25
*
WCL, anti-MMP9
F
Maker
Control si
MMP3 si
MMP9 si
MMP3/9 si
kD
250
150
100
75
50
37
25
*
Sup., gelatin zymo



Fig. S3